JOURNAL OF GEOPHYSICAL RESEARCH, VOL. 100, NO. D4, PAGES 7363–7379, APRIL 20, 1995

The annual cycle of stratospheric water vapor in a general circulation model

Philip W. Mote[1]

Department of Atmospheric Sciences, University of Washington, Seattle

Abstract. The application of general circulation models (GCMs) to stratospheric chemistry and transport both permits and requires a thorough investigation of stratospheric water vapor. The National Center for Atmospheric Research has redesigned its GCM, the Community Climate Model (CCM2), to enable studies of the chemistry and transport of tracers including water vapor; the importance of water vapor to the climate and chemistry of the stratosphere requires that it be better understood in the atmosphere and well represented in the model. In this study, methane is carried as a tracer and converted to water; this simple chemistry provides an adequate representation of the upper stratospheric water vapor source. The cold temperature bias in the winter polar stratosphere, which the CCM2 shares with other GCMs, produces excessive dehydration in the southern hemisphere, but this dry bias can be ameliorated by setting a minimum vapor pressure. The CCM2's water vapor distribution and seasonality compare favorably with observations in many respects, though seasonal variations including the upper stratospheric semiannual oscillation are generally too small. Southern polar dehydration affects midlatitude water vapor mixing ratios by a few tenths of a part per million, mostly after the demise of the vortex. The annual cycle of water vapor in the tropical and northern midlatitude lower stratosphere is dominated by drying at the tropical tropopause. Water vapor has a longer adjustment time than methane and had not reached equilibrium at the end of the 9 years simulated here.

1. Introduction

In the troposphere, water in all phases plays a crucial role in the energetics of atmospheric transport and in daily weather: its phase changes release latent heat, providing an internal energy source for circulations of all scales. In the stratosphere, where its concentration is orders of magnitude smaller and its turnover time is orders of magnitude longer, water vapor also plays a crucial role, though for different reasons. It plays a chemical role, for instance as a source of OH radicals which participate in most chemical cycles in the stratosphere, and a radiative role, as an absorber and emitter of infrared radiation and as an absorber of solar radiation. Water vapor is unique among long-lived trace gases in that it occasionally saturates under stratospheric conditions (Figure 1), and its saturation varies strongly with temperature, approximately a factor of 6 for a 10 K adiabatic temperature change.

The strong dependence of water vapor saturation on temperature is arguably the most interesting and useful attribute of water, from the standpoint of tracer studies; it has contributed in myriad ways to the advancement of our understanding of the middle atmosphere, as a brief historical overview shows. Prior to the late 1940s, it was generally assumed that the stratosphere was in radiative equilibrium and its composition affected only by turbulent diffusion which mixed species up from the troposphere [*Brewer*, 1949]. But in analyzing water vapor measurements over England, Brewer concluded that the observed mixing ratios were considerably lower than the minimum saturation mixing ratios at the local tropopause, while the upward diffusion model would imply mixing ratios equal to the local minimum saturation mixing ratio. He deduced that stratospheric air in midlatitudes must have entered the stratosphere in the tropics, where frost points were sufficiently low (190-195 K) to explain the observed mixing ratios.

The observed lower stratospheric water vapor mixing ratios imply a limited location and season of troposphere-stratosphere mass transfer [*Holton*, 1984], since temperatures must be low enough to remove nearly all water vapor by saturation (the "cold trap"). Thus although annual mean, zonal mean tropical tropopause temperatures are too warm to explain observed lower stratospheric water vapor mixing ratios, the cold trap condition is met at some times and locations. *Newell and Gould-Stewart* [1981], for instance, identified locations and times when tropical 100-hPa temperatures were low enough to explain the observed lower stratospheric mixing ratios.

In addition to identifying locations and times of stratosphere-troposphere exchange, the strong dependence of water vapor saturation on temperature has posed a great challenge to in situ measurements. Because water vapor mixing ratios are so much higher in the troposphere than in the stratosphere (1-10 parts per hundred, compared to 1-10 parts per million), even minute contamination of the instrument can overwhelm stratospheric measurements; after passage through the cold tropopause, much higher stratospheric temperatures can sublimate any condensate acquired on ascent and can raise measured vapor amounts considerably above the actual vapor amount. For example, *Kley et al.* [1979] found values exceed-

[1]Now at U.K. Universities' Global Atmospheric Modelling Programme (UGAMP) and Department of Meteorology, University of Edinburgh, Edinburgh, Scotland.

Paper number 94JD03301.
0148-0227/95/94JD-0330/$05.00

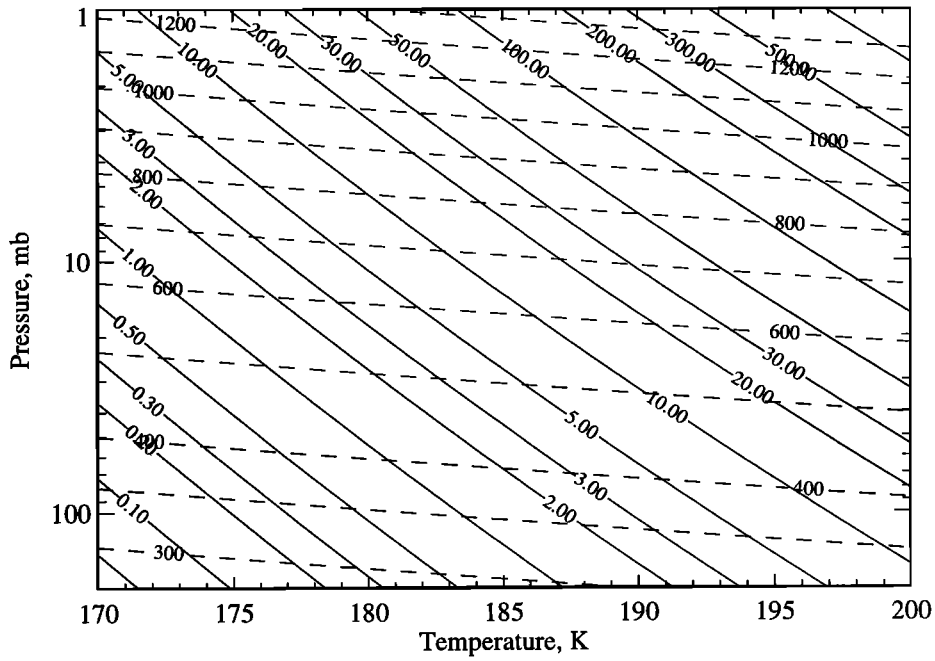

Figure 1. Saturation mixing ratio (parts per million by volume, solid contours) and potential temperature (Kelvin, dashed contours) for selected stratospheric pressures and temperatures.

ing 100 ppmv at 30 km and found that by increasing the flow rate through the instrument and by heating it for several minutes before descent, they could reduce peak mixing ratios by a factor of 10.

The measurements taken by remote methods, for instance, by rocket or ground-based radiometers, generally showed no increase of water vapor with height in the stratosphere. It was thus reasonable to doubt, as did *Ellsaesser* [1983], whether the increase with height measured by in situ methods was real or was an artifact of the outgassing problems mentioned above. Latitudinal variations were similarly difficult to deduce; *Harries'* [1976] comprehensive review indicated that lower stratospheric water vapor decreased with latitude.

Most such uncertainty and misconception was dispelled when the Nimbus 7 Limb Infrared Monitor of the Stratosphere (LIMS) conducted the first global, satellite-based measurements of stratospheric water vapor from October 1978 to May 1979 [*Russell et al.*, 1984, *Remsberg et al.*, 1984]. Results clearly showed that stratospheric water vapor had a minimum in the tropics which increased gradually poleward and upward. The upward increase in height was consistent with a photochemical source of water vapor from the destruction of methane, as was suggested by *Ellsaesser* [1974]. Measurements near the tropical tropopause have low accuracy [*Remsberg et al.*, 1990b], and the LIMS water vapor values there are both much lower and much less seasonally dependent than other observations indicate.

A series of ER-2 aircraft studies of stratospheric water vapor [*Kley et al.*, 1982, *Kelly et al.*, 1989, 1990, 1993] have focused on the two stratospheric regions where temperatures and pressures are favorable for saturation: the tropical tropopause and the polar vortices. The latter region has come under scrutiny since the discovery of dramatic, seasonal ozone depletion, while stratosphere-troposphere exchange takes place in the former region. The role of water vapor in ozone depletion is critical: condensation within the extremely cold polar vortex forms polar stratospheric clouds (PSCs), whose surfaces permit extremely fast heterogeneous chemical reactions to liberate chlorine from reservoir species; active chlorine then catalytically attacks ozone (see, for example, *Molina et al.* [1987]). PSCs generally contain not just water ice but also nitric acid trihydrate (NAT) or nitric acid dihydrate (NAD), which condense at slightly higher temperatures than water ice crystals.

Western hemisphere tropical measurements of lower stratospheric water vapor [*Mastenbrook*, 1968, 1974; *Kley et al.*, 1979, 1982] generally showed a minimum in water vapor that was above the tropopause and drier than the local minimum saturation, just as in mid-latitudes, implying a source at another location (or time). *Newell and Gould-Stewart* [1981] and *Robinson and Atticks Schoen* [1987] identified the most likely source of stratospheric dry air as the "maritime continent" region (near Indonesia) during northern winter. The tropical measurements of *Kelly et al.* [1993] conclusively showed that in this region, minimum mixing ratios were coincident with the local tropopause and low enough to explain observed low values at other times and locations.

While LIMS provided measurements for only 7 months, the Stratospheric Aerosol and Gas Experiment (SAGE II) has provided continuous measurements of stratospheric water vapor since 1985; results from 1985-1989 have recently been published [*Rind et al.*, 1993] and show interesting details of the seasonal and interannual variations which will be discussed below. The Upper Atmosphere Research Satellite (UARS), launched in September 1991, bore four instruments capable of measuring water vapor: the microwave limb sounder (MLS), improved stratospheric and mesospheric sounder (ISAMS), the halogen occultation experiment (HALOE), and the cryogenic limb array etalon spectrometer (CLAES). Preliminary water vapor results from UARS have already been published [*Harwood et al.*, 1993; *Mote et al.*, 1993; *Tuck et al.*, 1993].

The various observations mentioned above agree on some

aspects of the stratospheric water vapor distribution and time dependence. During most of the year, minimum mixing ratios occur at or just above the tropical tropopause and are larger in northern summer than northern winter. Mixing ratios increase upward and poleward, largely due to methane oxidation in the upper stratosphere. As a result of the seasonal cycle in both transport and tropical tropopause mixing ratios, the minimum in midlatitudes occurs in about March in both hemispheres [*Mastenbrook and Oltmans*, 1983; *McCormick et al.*, 1993].

But there are numerous puzzles about the observed water vapor distribution. The Brewer-Dobson model assumed that midlatitude lower stratospheric water vapor mixing ratios are directly influenced by air that has recently passed through the tropical tropopause; is it possible that some of this influence is polar, as was suggested by *Stanford* [1973] and *Tuck et al.* [1993]? What are the distribution and seasonal cycle of water vapor in the lower stratosphere, where satellite instruments have difficulty observing? Is the elevated hygropause, that is, the presence of a water vapor minimum above the local tropopause, indeed due to transport from a distant source region?

The purpose of this paper is to address some of these questions with a general circulation model (GCM), and also to outline some of the shortcomings of using a GCM to study stratospheric water vapor. Previous GCM studies of water vapor did not include methane photochemistry. *Allam and Tuck* [1984] discussed water vapor in their GCM, which had low vertical resolution (13 levels) and no water vapor source. *Le Texier et al.* [1988] used a two-dimensional (2-D) model and performed detailed photochemical calculations of water and many other species. In the lower stratosphere, however, the longitudinal dependence of stratosphere-troposphere exchange renders a 2-D model inadequate for studying water vapor. *Cariolle et al.* [1990] simulated the Antarctic ozone hole using a fairly high-resolution GCM but only showed lower stratospheric water vapor for that region and season, and they did not mention a stratospheric source of water vapor. *Rasch et al.* [1995] undertook a most ambitious effort: a thorough treatment of stratospheric chemistry and dynamics, representing about twenty trace constituents and several dozen reactions in a GCM. They included detailed water vapor photochemistry, and this work should be considered as complementary to theirs.

2. Description of the General Circulation Model

The general circulation model used in this study is the new version of the NCAR Community Climate Model (CCM2). The CCM2, a global spectral model, represents a complete redesign of the CCM and is ideally suited to the study of tracers in the stratosphere. It employs a semi-Lagrangian (SLT) scheme for constituent transport [*Rasch and Williamson*, 1991], a new convective mass flux approach to parameterized convection [*Hack*, 1994], and improved treatment of clouds and longwave and shortwave radiation. A complete description may be found in the work of *Hack et al.* [1993]. Momentum sinks above the boundary layer are provided both by parameterized gravity wave drag and by Rayleigh friction in the mesosphere.

This study used a middle atmospheric version of the CCM2 which extends vertically to about 75 km and has much finer vertical resolution than in the standard 19-level (L19) version of CCM2. The vertical resolutions used here were L35 with roughly 2.5 km spacing between levels in the middle atmosphere, L75 with roughly 1-km spacing, and L44 with roughly 1.5 km spacing. The L35 and L75 runs were performed using a horizontal resolution of triangular-31 (T31) resolution, approximately 3.75° x 3.75°, and the L44 run used a trapezoidal truncation (T42x21), approximately 2.8° x 5.6°. As the CCM2 was under development during this study, an earlier and a later version were used, called here v13 and v17.

A modeling study of middle atmospheric water vapor requires a representation of the methane source. This can be accomplished by specifying the production term, by carrying methane as a tracer and including some simple chemistry, or by including a large number of chemical species and reactions. I have taken the second approach, while *Rasch et al.* [1995] have adopted the third approach. Methane is a useful tracer for diagnosing the residual circulation of the model and for validating with satellite observations.

The chemistry of methane oxidation with respect to water falls between two extremes [*Remsberg et al.*, 1984]:

$$CH_4 + 3.5O_2 + h\nu \Rightarrow 1.5H_2O + CO + 0.5H_2 + 1.5O_3 \quad (1)$$

$$CH_4 + 3O_2 + h\nu \Rightarrow 2H_2O + CO + O_3 \quad (2)$$

that is, between 1.5 and 2.0 water molecules produced per methane molecule oxidized. With respect to the tracers considered here, these equations can be simplified as

$$CH_4 + h\nu \Rightarrow \beta H_2O \quad (3)$$

The 2-D modeling results of *Le Texier et al.* [1988] and an analysis of both LIMS (H_2O) and SAMS (CH_4) observations [*Hansen and Robinson*, 1989] indicate that the value of β increases with height in the stratosphere, reaching values close to 2 at the stratopause. At this altitude the photodissociation of methane is most efficient; for this reason and because some H_2 in (1) is ultimately converted to water vapor, in this study β is set to 2, overestimating (by perhaps 10%) the equilibrium amount of stratospheric water vapor. The value of β was doubled for part of year 4 to speed the moistening of the stratosphere. The methane mixing ratio was fixed at 1.5 ppmv in the lower troposphere, a lower value than is presently observed. In the stratosphere, the initial distribution of methane was taken from a simulation using the 2-D model of *Garcia and Solomon* [1983]; the rate constants for reaction (3) were also taken from their model and are functions of latitude, height, and month.

Water vapor is completely determined by model processes (including, in this case, methane oxidation) and interacts with radiation. The initial condition for water vapor, as for other dynamic fields, was output from a multiyear T31, v13 run. The stratosphere was quite dry, with values below 1 ppmv in the upper stratosphere and about 2.5 ppmv in the lower stratosphere.

A time line of the integrations performed in this study is illustrated in Figure 2. All major runs began and ended on September 1. Most of the discussion below will focus on the 4-year simulations at T31L35 (run A) and T42x21L44 (run B), which differed in many respects, not just resolution. Run A used CCM2 v13, while run B used v17; radiative calculations were done half as often in run B, and Rayleigh friction was greater above 50 km in run B. The 180-day "control" and "no-dehydration" runs, which are discussed in section 5, used

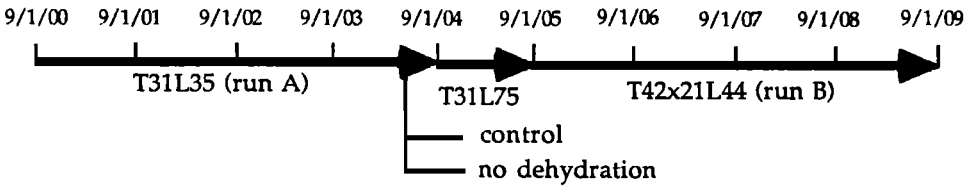

Figure 2. Time line of CCM2 simulations. Dates are shown from September 1 year 0 (9/1/00) to September 1 year 9 (9/1/09). Heavy arrows denote major model runs, with resolution indicated below the arrow.

T31L35 resolution and v17 and were initialized on June 1 of the fourth year of run A.

The CCM2, like other GCMs, suffers from a cold polar bias which is particularly acute in the southern winter middle stratosphere; temperature errors can exceed 40 K and are arguably due to deficiencies in the gravity wave drag [*Garcia and Boville,* 1995]. The temperatures reached (<170 K) are sufficiently cold to reduce mixing ratios to a few tenths of a part per million, and the cold bias produces condensation at altitudes much higher than observed (see section 5). As a partial remedy to this cold bias, the saturation vapor calculation in the CCM2 includes a dehydration limiter which operates as follows: for temperatures below a critical value T_{min}, the saturation vapor pressure $e_s(T)$ is set to $e_s(T_{min})$. The default value of T_{min} is 173 K, but raising it to 181 K (as was done in tests and in run B) limits dehydration. For the very low mixing ratios in the stratosphere, the mixing ratio is roughly proportional to the vapor pressure divided by the ambient pressure. Consequently, the higher value of T_{min} has greatest impact at lower pressures, which is, conveniently, where the greatest temperature bias in the CCM2 occurs. Six-month test runs with the two values of T_{min} are dynamically similar.

3. Transient Adjustment of the Model Stratosphere to Water Vapor Sources

In general, the distribution of a tracer in the atmosphere reflects an approximate balance between transport and the sources and sinks of the tracer. If the tracer distribution is initially out of balance, the system tends to restore the balance. The duration of this transient adjustment depends on the magnitude of the initial imbalance and on the characteristics of the transport and the sources and sinks, and thus provides an indicator of response times to arbitrary changes, such as enhanced surface flux (for surface-source tracers) or a reorganization of the circulation.

The moistening of an initially dry middle atmosphere takes many years, as does the adjustment of total stratospheric methane to the CCM2 circulation. A consideration of tracer budgets permits one to quantify response times. The general form of the tracer continuity equation is

$$D\chi / Dt = S \tag{4}$$

where χ is the tracer mixing ratio,

$$\frac{D}{Dt} = \frac{\partial}{\partial t} + \frac{u}{a\cos\phi}\frac{\partial}{\partial \lambda} + \frac{v}{a}\frac{\partial}{\partial \phi} + \omega\frac{\partial}{\partial p}$$

is the substantial derivative in spherical, pressure coordinates, and S is the combined source/sink term. Using the continuity equation, (4) can be rewritten in flux form as

$$\frac{\partial}{\partial t}(\chi) + \frac{1}{a\cos\phi}\frac{\partial}{\partial \lambda}(u\chi) + \frac{1}{a}\frac{\partial}{\partial \phi}(v\chi) + \frac{\partial}{\partial p}(\omega\chi) = S \tag{5}$$

Integrating over the whole globe and from pressure p_0 to the top of the model p_t, where ω=0, gives

$$\frac{\partial}{\partial t}\{\chi\} = -[\omega\chi]\Big|_{p_0} + \{S\} \tag{6}$$

where $\{\chi\} = \int_{p_t}^{p_0}[\chi]dp$ and $[\chi]$ denotes a global average on a pressure surface. The forms of equation (6) for water vapor and methane are

$$\frac{\partial}{\partial t}\{CH_4\} = -[\omega CH_4]\Big|_{p_0} - \{rCH_4\} \tag{7a}$$

$$\frac{\partial}{\partial t}\{H_2O\} = -[\omega H_2O]\Big|_{p_0} + \beta\{rCH_4\} - L \tag{7b}$$

where $r=r(\phi,z,t)$ and β are the methane loss rate and conversion efficiency, respectively (see section 2). The term L represents water vapor loss due to condensation.

It is then possible to associate a time scale with each process. For the total tracer $\{\chi\}$ above a level p_0, the time scale τ of a process represented by a term ζ on the right-hand side of equations 7a and 7b is simply

$$\tau = \{\chi\}/|\zeta|. \tag{8}$$

The timescales of the processes ζ are summarized in Table 1 for year 4 of run A with p_0 =49 hPa. The two tracers still have not reached equilibrium, and their tendencies are nonzero.

The long times in Table 1 imply that middle and upper stratospheric methane will be approaching equilibrium after the 9 years of simulation here, but water vapor will take longer to come to equilibrium. As the total tracer $\{\chi\}$ approaches equilibrium, the left side of equation (6) goes to zero and the two terms on the right become equal in magnitude; consequently the times τ represented in Table 1 would also become equal for each tracer and would fall between the values calculated when the tracer is out of equilibrium.

It would be instructive to examine the evolution of the water vapor field from a dry stratosphere to the beginning of this

Table 1. Timescales (years) for Tracer Changes Above 49 hPa

	Source/Sink	Net Flux
Methane	10.3	7.3
Water Vapor	14.0	37.2

run, in order to study the influence of dynamics in the absence of the methane source. Unfortunately, it is impossible to reconstruct a history of the water vapor field because the ancestral model runs have been deleted; the transient process of balancing equation (7b) without a methane source cannot be observed.

It is, however, possible to examine the response of total stratospheric water and methane for the 9 years of integration performed for this experiment. Because the vertical resolution changes, the $\{\chi\}$ term in equation (6) is better represented as a mean mixing ratio than as a total mass. The values of p_0 chosen here, 100 hPa, 25 hPa, and 1 hPa, are representative of the lower and upper stratosphere and of the mesosphere, respectively, and also fall relatively close to model levels at all three resolutions. The two processes represented in equation 6, net advection through the pressure surface p_0 and chemical destruction or production above p_0, are time-dependent and the former in fact depends upon the balance of transport and chemistry below p_0.

Figure 3 shows the globally averaged, mass-weighted mean water vapor mixing ratio above these levels for 9 years, and of methane above 25 hPa. A gradual increase is evident in the lower stratosphere (Figure 3a) between year 2 and year 7; in the last 2 years, changes in total stratospheric water are quite small. The increase in total water modulates a weak annual cycle whose minimum occurs in January and maximum in September. In the upper stratosphere (Figure 3b), water increases fairly steadily throughout the run and has not reached equilibrium at the end of 9 years, consistent with Table 1. A barely perceptible annual cycle has a minimum in August. In the mesosphere (Figure 3c), equilibrium appears to be reached after 4 years, but in the seventh year, water vapor again begins to increase. A weak semiannual oscillation is present.

Methane equilibrates more rapidly than water vapor but re-

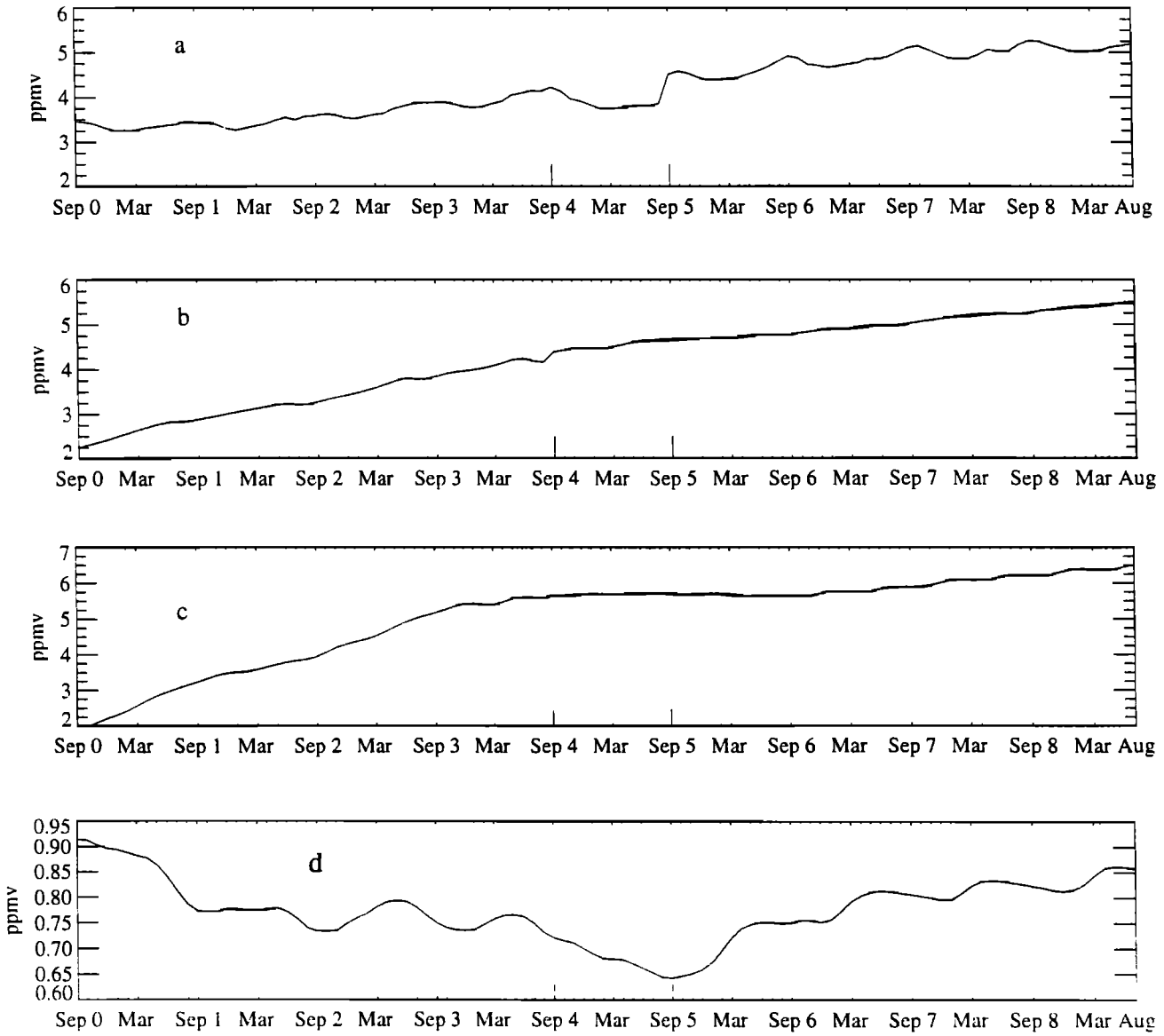

Figure 3. Global mean mixing ratio above different levels for 9 years of CCM2 runs: (a) water vapor above 100 hPa; (b) water vapor above 25 hPa; (c) water vapor above 1 hPa; (d) methane above 25 hPa. Resolution changes (see Figure 2) are indicated by vertical lines.

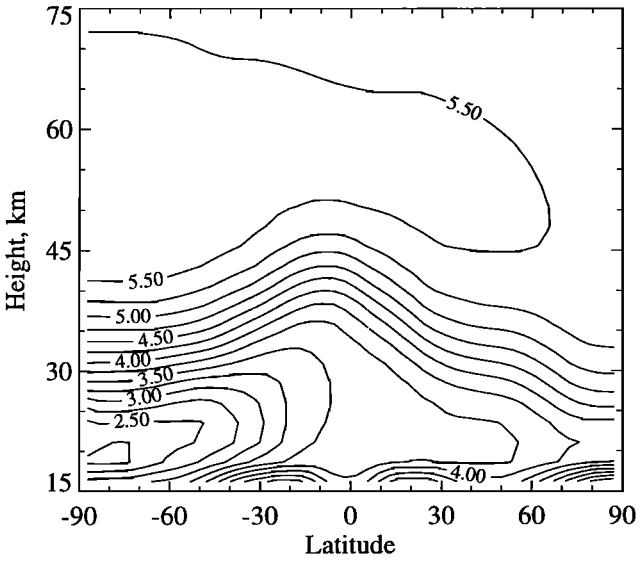

Figure 4. Zonal mean water vapor mixing ratio in January year 4, run A. Contour interval is 0.25 ppmv.

sponds more dramatically to the T31L75 resolution (Figure 3d). The chemical lifetime of methane decreases markedly with height in the stratosphere, and consequently methane equilibration times do as well. In the lower stratosphere (not shown), equilibration time is greater than 4 years, and the trend is downward throughout run A (years 1-4) and upward throughout run B (years 6-9). An abrupt sign change of the tendency of $\{\chi\}$ can only be due to the first term in (7a), since the second depends only on $\{\chi\}$; we can infer therefore that the methane (and mass) flux at 100 hPa in run B exceeds that in run A. In the upper stratosphere (Figure 3d) and the mesosphere, the equilibration time is much more rapid, 2 or 3 years for the upper stratosphere and about one year for the mesosphere. At greater altitudes the annual cycle, including a significant semi-annual component in the mesosphere, becomes evident.

The trends in methane and water vapor are large enough to mask features of the annual cycle, and where indicated, figures shown below have had a linear trend removed. The trend is calculated by finding the best fit line, subtracting the linear time-varying component from the time series, and then adding the value at the ending point. The last step ensures that the annual and interannual variations shown in these figures reflect variations about the final state, which is closest to equilibrium.

4. Annual Cycle of Stratospheric Water Vapor and Methane

Figure 4 shows the zonal mean water vapor concentration for the fourth January of run A. The significant features are a broad maximum in the upper stratosphere and lower mesosphere, an upward bulge of dry air in the tropical middle stratosphere, and in the lower stratosphere, a minimum in the lower stratosphere which increases monotonically from south to north. The lowest mixing ratio, 2.2 parts per million by volume (ppmv), occurs in the southern polar lower stratosphere.

Observed January mean water vapor mixing ratios from various global satellite data sets (see section 1) are shown in Figure 5. *Chiou et al.* [1993] have compared the LIMS and SAGE II water vapor data; for the present discussion their similarities are of more interest than their differences. All of the satellite observations (including unpublished UARS data) agree that there is a tropical minimum of 2-3.5 ppmv, and that mixing ratios increase upward and poleward, reaching a maximum at stratopause level of 6-8 ppmv. The CCM2 satisfactorily reproduces observed water vapor in the upper stratosphere, but is completely different from the observations in the lower stratosphere for run A.

The differences in the lower stratosphere between model and observations can be traced to two regions where saturation occurs and temperature errors are magnified: the tropical tropopause, where very low temperatures are too rare in the model, and the southern polar vortex, where very low temperatures are all too common in the model. At this resolution the CCM2 produces no closed contours around the tropical minimum, and instead, the minimum water vapor mixing ratio occurs in the southern polar lower stratosphere, even in January. The reasons for the first discrepancy have been discussed by *Mote et al.* [1994]; briefly, there is too little mass transport into the stratosphere under low mixing ratio conditions for three reasons. First, the vertical temperature minimum is constrained

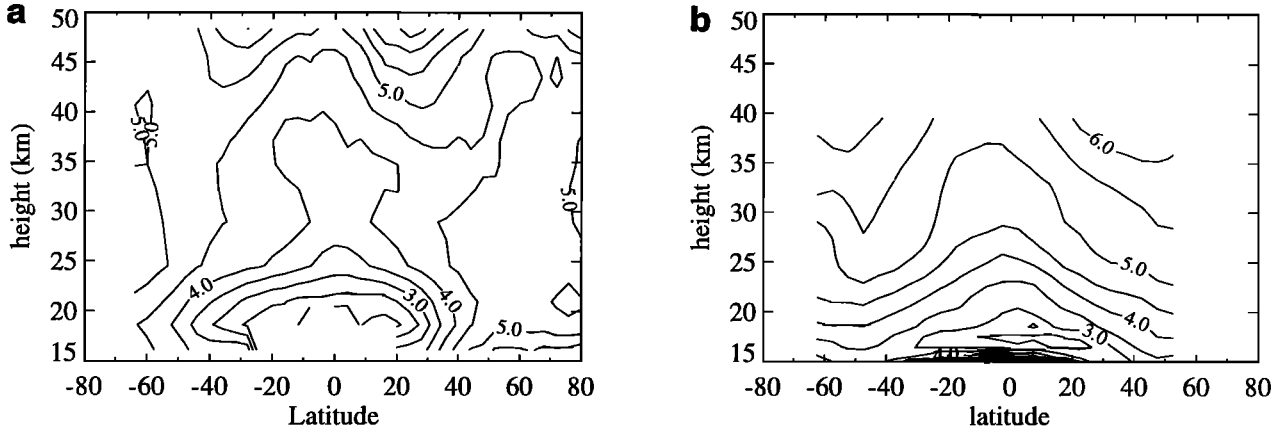

Figure 5. As in Figure 4 but for (a) LIMS in January 1979 (from the archived LIMS LAMAT data set [*Remsberg et al.*, 1990a]), (b) SAGE II January 1986-1991 mean [provided by E.-W. Chiou; see *McCormick and Chiou*, 1994]. Contour interval is 0.5 ppmv.

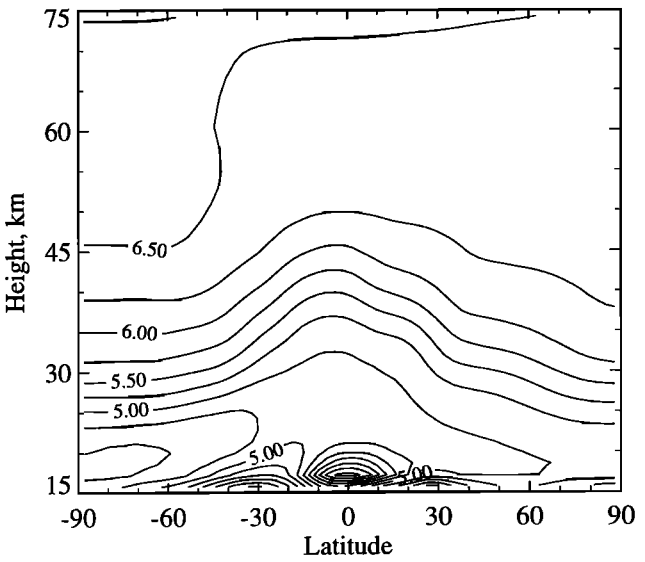

Figure 6. As in Figure 4 but for year 9 (run B).

to occur at a model level, which at L35 resolution produces a minimum at 99 hPa; observed minima, especially in the "stratospheric fountain" region, tend to occur at lower pressures [*Frederick and Douglass,* 1983; *Selkirk,* 1993]. Second, resolved-scale circulations produce excessive vertical mixing. Third, the time variance of temperature appears to be too small in the model; extreme values occur too seldom.

Run B included nonphysical solutions to these two problems. One solution is finer vertical resolution in the lower stratosphere, which permits the tropopause to form at 86 hPa and partly compensates for the three inadequacies listed above by reducing the mean tropopause temperature. The second problem can be addressed by raising the minimum saturation vapor pressure as was discussed in section 2. Run B also included enhanced Rayleigh friction in the upper stratosphere, which warms the southern polar region.

Figure 6 shows the impacts these alterations have on the zonal mean water vapor distribution in January. In the tropics, closed contours now appear around a considerably drier minimum, while the remnants of polar dehydration are less influential. This may be compared with Figure 4, and it can be seen that Figure 6 more closely resembles LIMS and SAGE II observations, in that the effects of polar dehydration are considerably diminished and the tropical minimum is enhanced.

The seasonal cycle can be seen in time series of monthly, zonal means of the two tracers. The following discussion will focus on run B, since it is tuned to produce a somewhat better simulation than run A. Figure 7 shows zonal mean, monthly mean 86-hPa water vapor plotted as a function of time and latitude for the 4 years of run B. Water vapor is strongly affected by saturation at this level and shows rather complex behavior. In the southern winter and early spring, thorough dehydration within the polar vortex dominates the high-latitude water vapor distribution. In the tropics, a minimum somewhat less than 3.5 ppmv appears in about January each year as tropopause temperatures decrease to their lowest values, in agreement with studies using radiosonde data [e.g., *Newell and Gould-Stewart,* 1981]. A curious feature develops in the subtropics each year in April-August, peaking in September or October: a maximum of around 6 ppmv, which indicates considerable flux from the troposphere at high local saturation mixing ratios. The cause of this feature is unclear.

The run A annual cycle at 99 hPa (not shown) is substantially the same as the run B annual cycle at 86 hPa. The chief differences are that in run A, mixing ratios are higher in the tropics and lower in southern midlatitudes, and that in northern hemisphere high latitudes, both water vapor and methane increase during winter. This increase suggest some influence of tropospheric air and extends to about 20 km and seems to be due to stationary eddies which are not as pronounced in run B.

In the middle stratosphere, water vapor has a simpler annual cycle than in the lower stratosphere, and differences between the two simulations are more pronounced. In run B (Figure 8a) the minimum tropical water vapor is approximately Sun-synchronous, reaching its maximum southward position (about 30°S) in February and its maximum northward position (0°) in July. At high latitudes in winter, water vapor increases due to subsidence, though in the southern hemisphere the seasonal dehydration masks the increase after May. Methane (Figure 8b) lags water vapor by about 3 months in the tropics and closely resembles its counterpart in run A (not shown); note also the high-latitude wintertime decrease.

In run A (Figure 8c), however, there is little annual cycle except in the southern middle and high latitudes; water vapor is dominated by a south-north gradient and by dehydration in southern winter high latitudes. During southern hemisphere

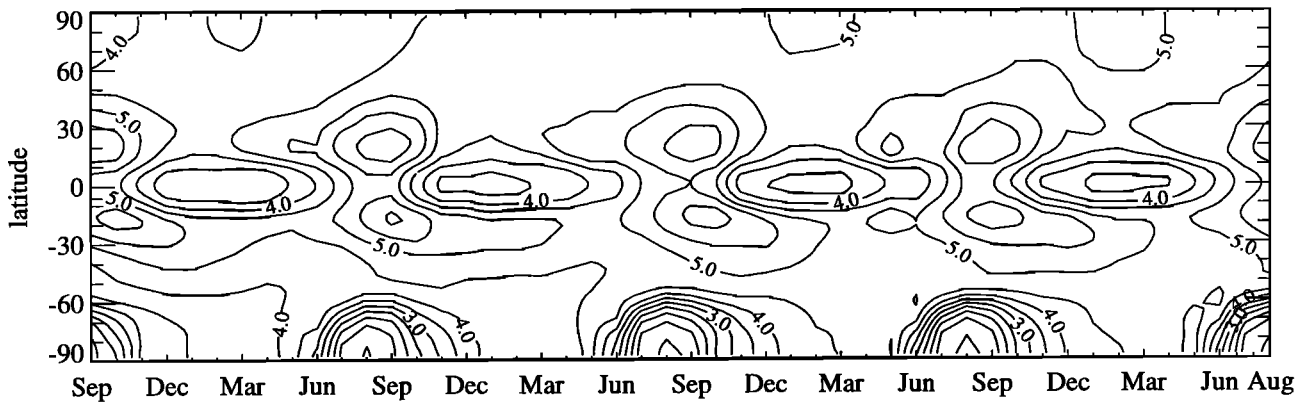

Figure 7. Time-latitude plot of zonal mean water vapor (parts per million by volume) at 86 hPa for run B. Contour interval is 0.5 ppmv.

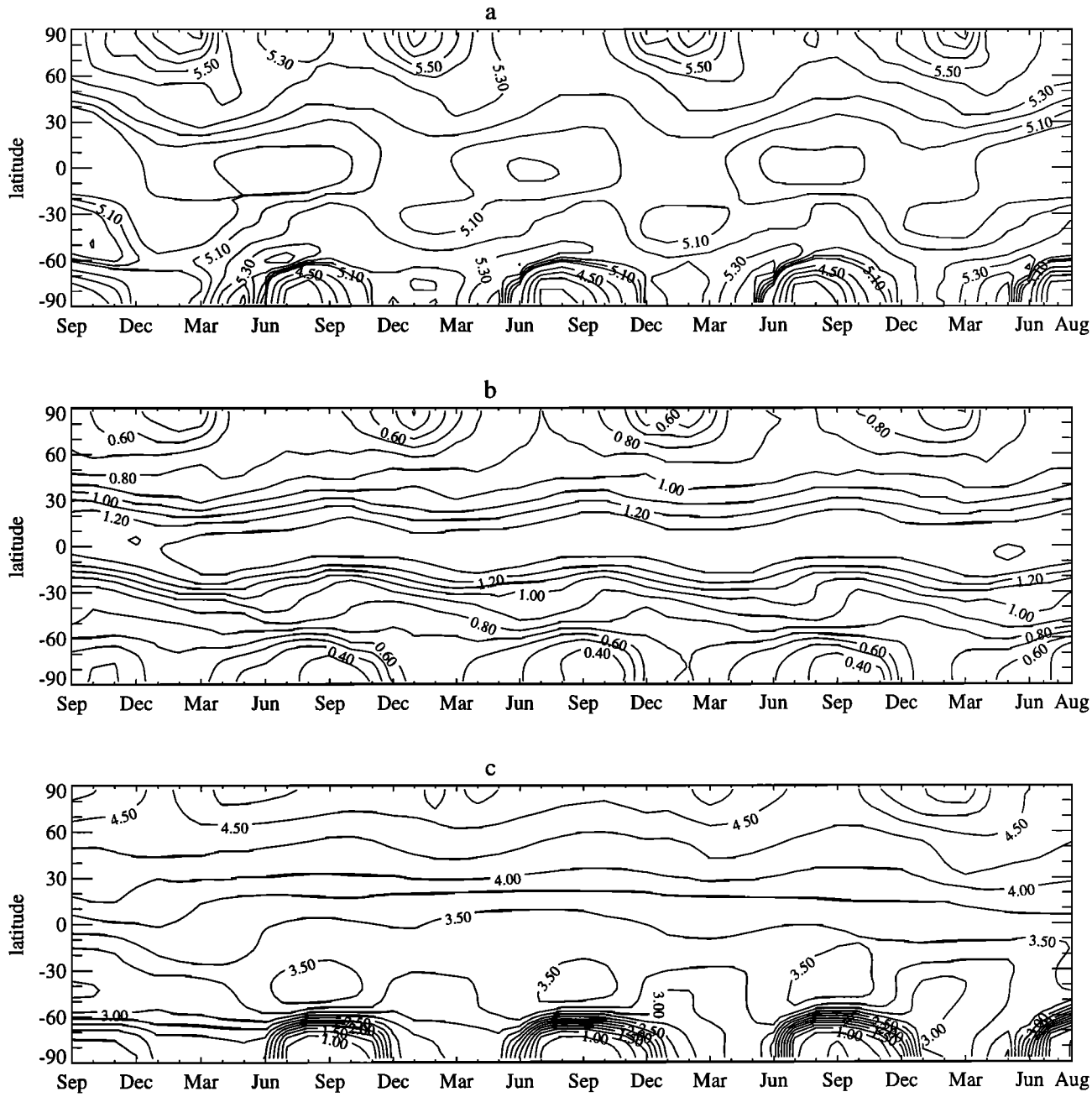

Figure 8. Time-latitude plot of 25 hPa zonal means, in parts per million by volume: (a) detrended water vapor, run B, with contour interval 0.5 ppmv below 5 ppmv, 0.1 ppmv above; (b) methane, run B, contour interval 0.1 ppmv; (c) detrended water vapor, run A, contour interval 0.25 ppmv.

late winter a water vapor maximum appears at about 50°S due to subsidence outside the vortex, as is suggested by the concomitant decrease in methane (not shown, but see Figure 8b). Polar dehydration is considerably greater; minimum mixing ratios are less than 0.5 ppmv, compared to more than 2 ppmv in run B. For run A the water vapor annual cycle is similar between 24 hPa and 10 hPa, with a south-north gradient, but above that, water vapor is dominated entirely by the trend and the two hemispheres are nearly symmetric.

In midlatitudes, observations [*McCormick et al.*, 1993] show a minimum mixing ratio appearing in February or March in each hemisphere at about 16 km. The simultaneity of the minimum in both hemispheres indicates tropical control, since minimum tropical mixing ratios occur 1-2 months earlier. Above and below the minimum, isopleths rise and fall seasonally, being lowest in winter and highest in summer. The seasonal cycle of midlatitude water vapor in the CCM2 shows rising and falling isopleths as observed (Figure 9). The northern hemisphere annual cycle in profile minimum water vapor is too high (19 km versus 16 km) and too weak (roughly 0.3 ppmv versus 1 ppmv) for run B compared to observations. In the southern hemisphere, the midlatitude profile minimum occurs quite high (23 km) and may be due to polar, not tropical, dehydration. In run A, a March minimum occurs only in southern midlatitudes; in northern midlatitudes, no annual minimum appears, and the monotonic increase with time is the

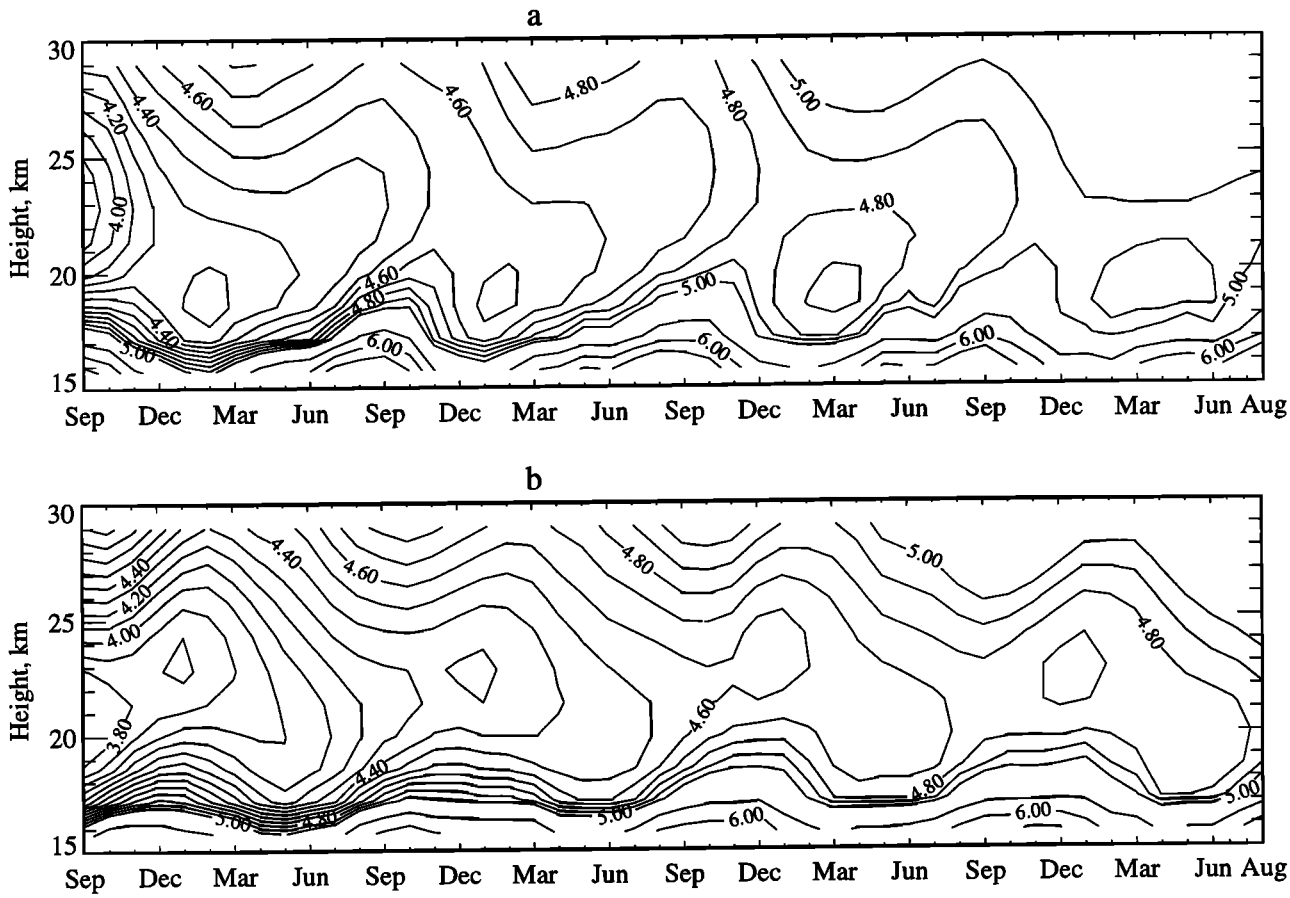

Figure 9. Time-height plot of average water vapor mixing ratio at (a) 30°N to 40°N, and (b) 30°S to 40°S, for run B.

dominant feature throughout the stratosphere. Tropical minimum mixing ratios are too high in run A to produce seasonal variations in midlatitudes, and even in run B, the annual minimum in the tropics has much less influence on midlatitudes than in the observations.

Tropical dry air does, however, have an influence in the vertical in the CCM2. Figure 10 shows that the annual minimum and maximum in tropical tropopause water vapor clearly propagate upward at a rate of about 2 km/month to about 30 km, where the signal is lost. Recent studies [*Mote et al.*, 1995] using water vapor observations from the MLS and HALOE instruments aboard UARS show the same sort of feature.

5. Dehydration in the Southern Polar Vortex

The obvious explanation for the dry swath in the southern hemisphere in Figure 4 is that the cold bias of the CCM2 at high latitudes causes excessive dehydration in southern hemisphere winter, and this dry air spreads equatorward. In this section it is shown that this is the correct explanation and also that air dried in the polar vortex can affect midlatitudes in a simulation that more closely resembles the observed atmosphere (run B).

In the CCM2, condensed water immediately falls as precipitation. The stable condensation term of the water vapor continuity equation may be used as a surrogate for polar stratospheric clouds (PSCs). When this term is nonzero in the polar stratosphere, it can be assumed that PSCs should be present. A major difference between condensation in the model and in the atmosphere is that cloud ice cannot re-evaporate in the model, so that PSCs produce exaggerated drying.

Comparison of Extent and Duration of Polar Stratospheric Clouds: Modelled and Observed

The SAM II instrument observed PSCs between June 24 and September 29 in 1979 [*McCormick et al.*, 1982] and between June 6 and October 24 in 1987, though they were probably present in late May [*Watterson and Tuck*, 1989, hereinafter WT]. In the CCM2, condensation also occurs from early June to late October; there is some variation from year to year and between runs. Figure 11 shows condensation at 70 hPa during the control simulation; condensation is present at this level from approximately June 10 to October 3 and weakens with time. The duration of condensation decreases with height, beginning somewhat later and ending much earlier. Variability on short time scales is large in Figure 11 and dehydration events are associated with rapid (2-4 days) bursts of eddy kinetic energy, indicating that synoptic-scale waves play an important role in dehydration as suggested by *Tuck* [1989].

The vertical extent of PSCs is much greater in the model than in observations due to the increasing cold bias with height. Whereas *McCormick et al.* [1982] and WT reported most clouds occurring below about 24 km in SAM II data, in the CCM2 condensation occurs as high as 4 hPa (38 km) in the control run and run A. In run B it only extends to about 20 hPa (27 km). Figure 12 shows the seasonal cycle of water vapor

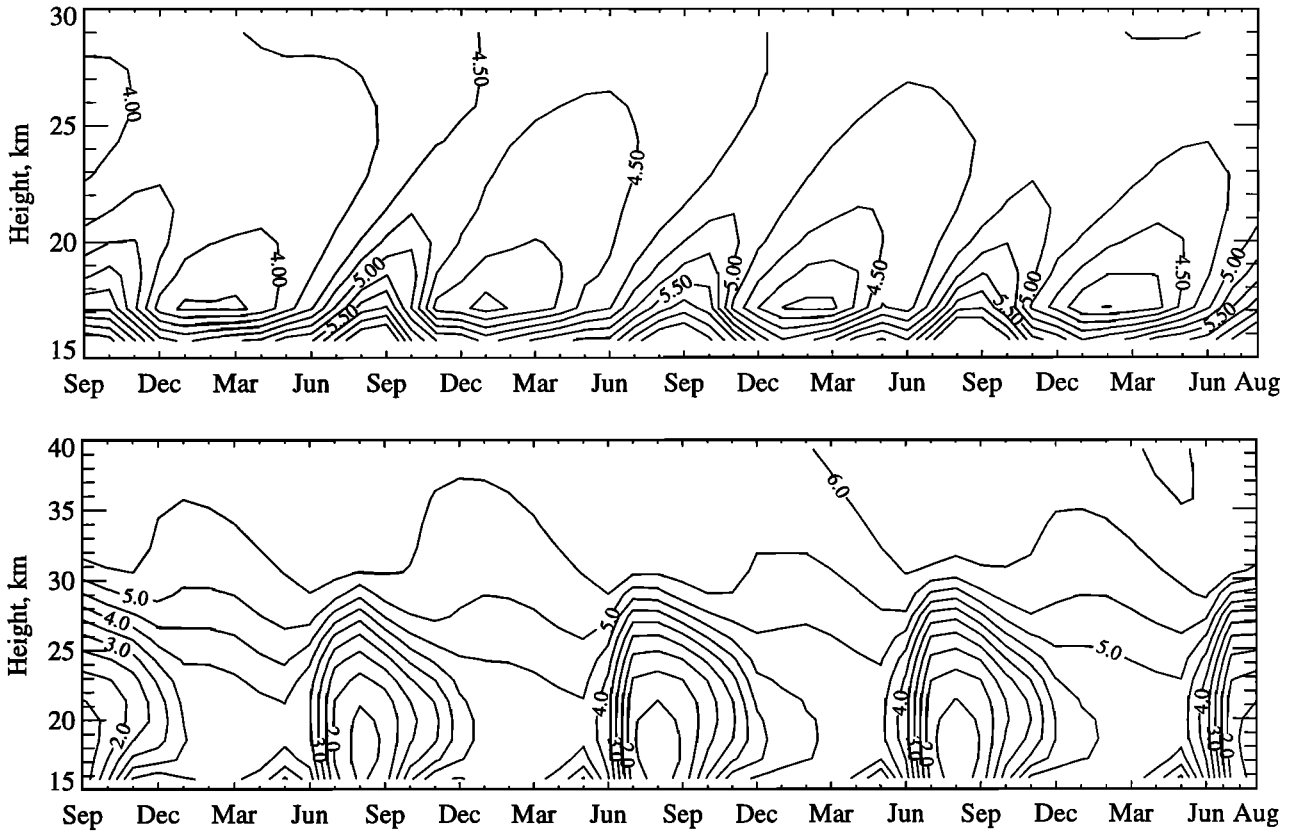

Figure 10. Time-height plot of average water vapor mixing ratio between 20°S and 20°N, run B.

over Antarctica with the annual minimum in August and maximum in May. Wintertime descent occurs from March to October, though its signal is clearer in methane (not shown).

The longitudinal distribution of PSCs is well simulated in the CCM2; Figure 13 shows a peak at about 120°W with most cloud occurring between 30°W and 180°. Initial dehydration occurs between 120°W and 180°, at latitudes not observed by SAM II, and later in the period condensation is confined to 30°-90°W. In mid to late winter, WT also found most cloud occurring in the western hemisphere with a peak over the Antarctic peninsula. Maximum condensation does not coincide with minimum temperature because condensation requires both low temperatures and adequate water vapor. As is shown by WT and by Figure 11, the early depletion of water vapor in the center of the vortex inhibits further condensation there, while condensation continues at the edge of the vortex where water vapor is more readily available.

Influence of Polar Dehydration on Midlatitudes

The idea that dehydration in the southern polar region might be of significance to the stratospheric water vapor budget was first put forth by *Stanford* [1973]. *Ellsaesser* [1974] attempted to calculate the water vapor budget for the strato-

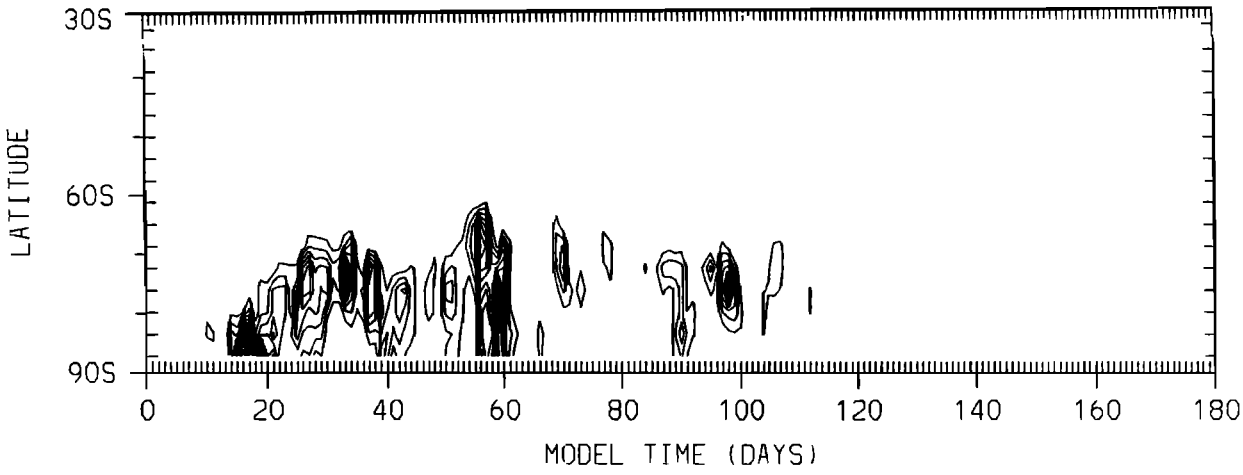

Figure 11. Evolution of zonal mean condensation at 70 hPa for the 180-day control simulation. Day 0 is June 1.

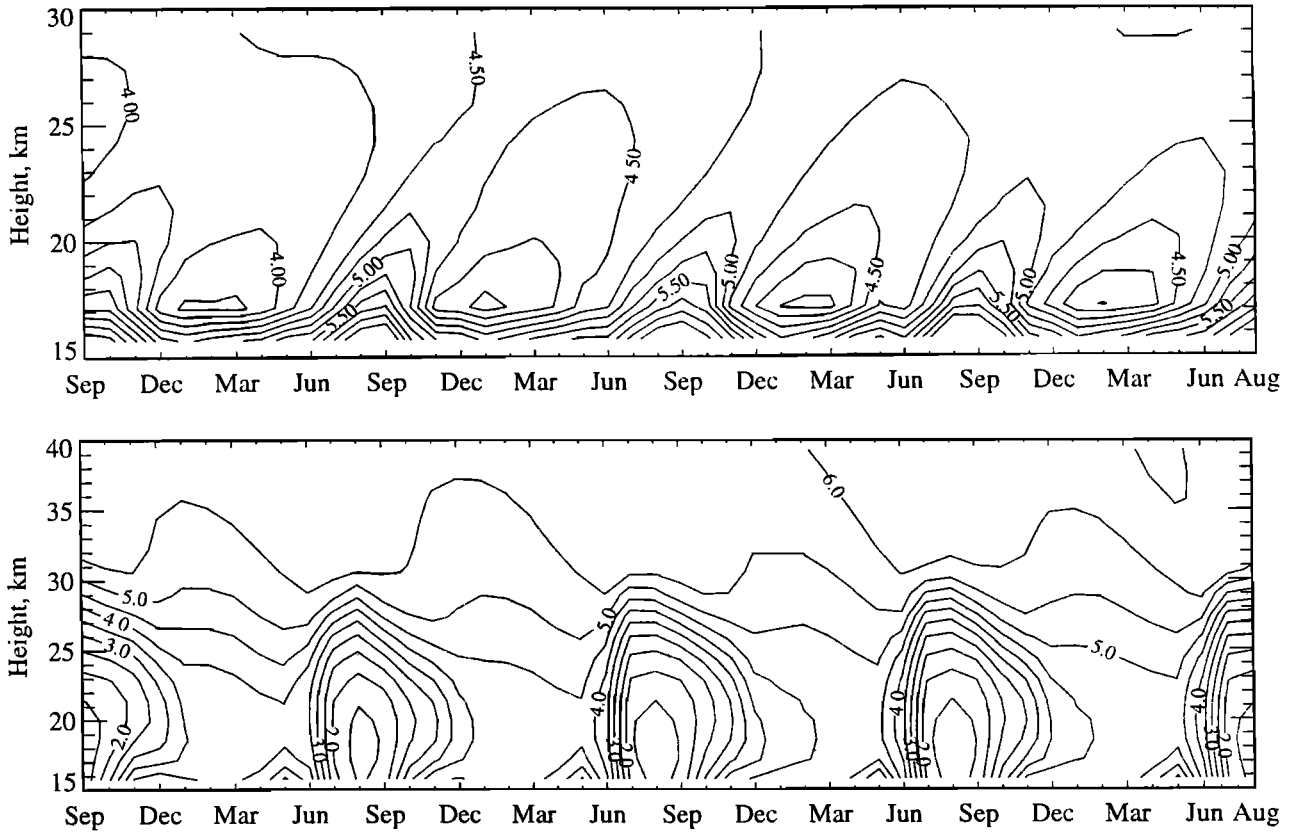

Figure 12. Time-height plot of average water vapor mixing ratio south of 70°S, run B.

sphere by assuming influx and outflux mixing ratios of 4 and 2.6 ppmm (5.5 and 4.2 ppmv), respectively, from *Mastenbrook's* [1968] balloon soundings. To remove the excess, he postulated a massive sink of water in the winter polar stratosphere. *Harries* [1976] criticized Ellsaesser for taking Mastenbrook's observations as representative of the entire tropopause and for ignoring the uncertainties; *Ellsaesser* [1977, 1983] defended his assumptions without rebutting Harries' criticism and clung to the notion of a massive polar sink of water.

Global observations, however, have not settled the question. LIMS did not observe the atmosphere during the period of active dehydration in the southern hemisphere lower stratosphere. SAGE II data faintly suggested that dehydration over Antarctica had some influence on midlatitude water vapor, as October zonal mean mixing ratios were slightly lower than April values below 18 km [*Rind et al.*, 1993]. The published SAGE data, however, do not extend poleward of 60°S. *Kelly et al.* [1989] showed that dehydration to 1.5 ppmv was occurring in conjunction with PSCs, and though air just outside the polar vortex had much higher water mixing ratios (3-4.5 ppmv), they argued that dehydration was affecting midlatitudes. *Kelly et al.* [1990] found that air just outside the southern hemisphere polar vortex was considerably drier than air outside the northern hemisphere polar vortex. Figure 14 shows global lower stratospheric water vapor data collected by the ER-2 research aircraft; the striking south-to-north gradient could certainly be due to a strong sink in the southern hemisphere polar vortex. Equatorward of 40°, there is no significant difference between the two hemispheres, indicating a limited impact of polar dehydration.

Observations of the zonal mean water vapor distribution by the HALOE instrument aboard UARS in southern spring 1992, however, showed evidence of possible influence of polar dehydration on midlatitude mixing ratios [*Tuck et al.*, 1993, *Mote et al.*, 1993]. M. Schoeberl (personal communication, 1993), however, doubts that this is true earlier in the year, since the polar vortex has only a fraction of the mass of a hemisphere. Modifying the mixing ratios in midlatitudes by 1-2 ppmv would require either a large mass flux through the polar vortex or considerable wave mixing, either of which would warm the vortex much more than observed. In the CCM2, however, polar dehydration certainly appears to influence midlatitudes (see Figure 4) even though the polar stratosphere is quite cold. If the model accurately represents the atmosphere, determining whether the model's polar dehydration affects midlatitudes would substantiate polar influence on observed midlatitude mixing ratios.

The question about the model's polar dehydration affecting midlatitudes can be addressed with two short simulations. Both were initialized on June 1 of the fourth year of run A (Figure 2), and the only difference between the two was that in one, condensation was not permitted in the stratosphere. Without dehydration, water vapor in the polar region (Figure 15) increases by about 1 ppmv during the 180-day run due to subsidence from the moist upper stratosphere. With dehydration, half the water in the column disappears within 2 months, when the difference between the two cases is greatest, and after that, water vapor slowly recovers.

The depletion of water in the polar vortex clearly impacts midlatitudes. The seasonal increase in water evident in the no-dehydration case, which may be due to increases in tropical

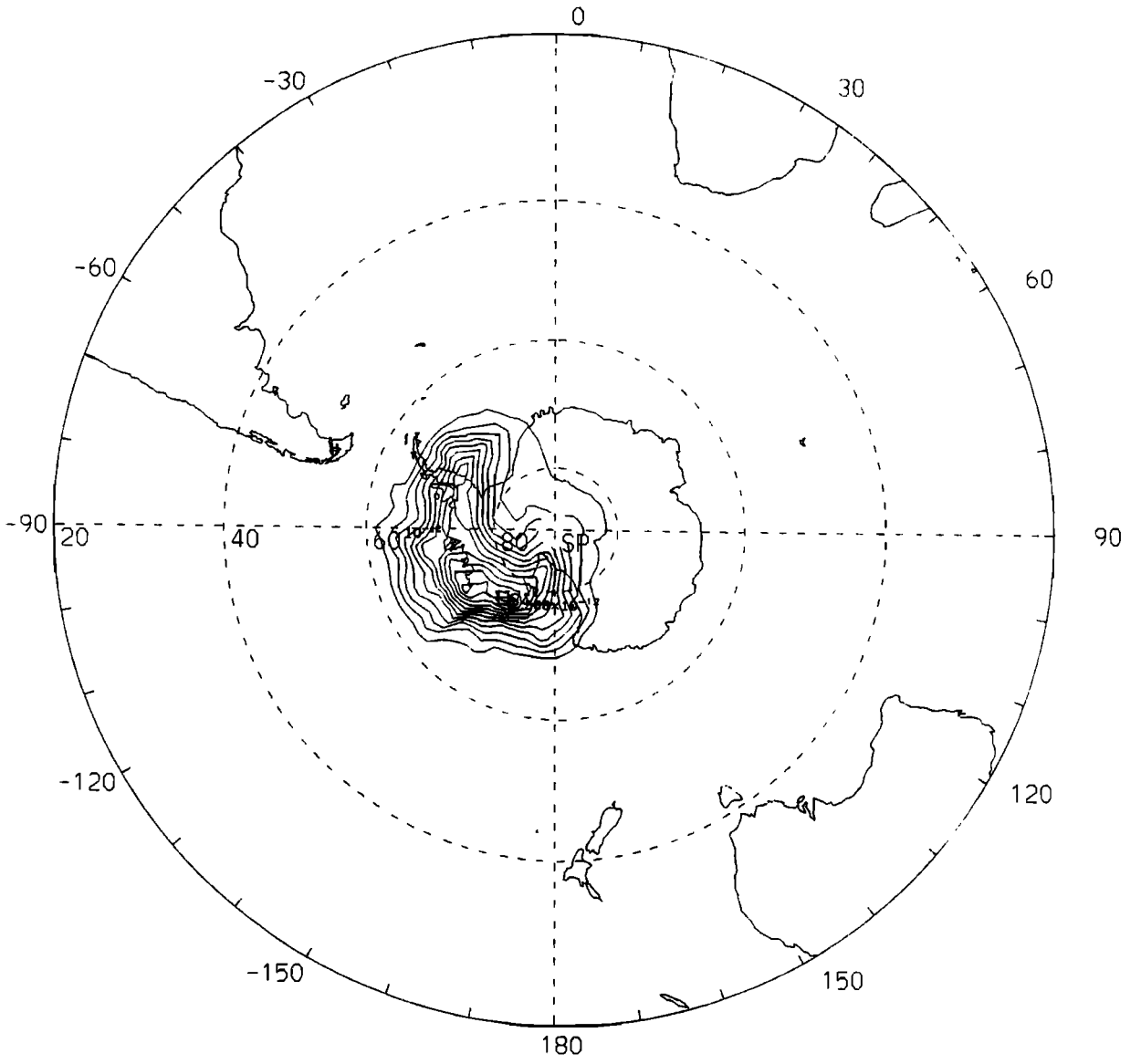

Figure 13. Condensation at 70 hPa, averaged over days 0-120 of the 180-day control simulation.

water vapor, is almost exactly balanced by polar dehydration in the control case, so that the mean mixing ratio remains constant at around 3.6 ppmv while the difference between the cases grows with time. The mass of air in the region 30°-60°S is about three times that in 60°-90°S.

In the tropics (not shown), the difference between the two cases is less pronounced than in midlatitudes, at most 0.25 ppmv, and is not apparent until the middle of the run. The circulation in the two cases is somewhat different, so it is not certain that the small difference in tropical water vapor is due to direct influence of dry air from the poles.

To understand the roles of various processes in producing the features noted above, it is instructive to consider the water vapor budget in the stratosphere. The transformed-Eulerian mean (TEM) tracer transport equation is [*Andrews et al.*, 1987, p. 357]

$$\frac{\partial \overline{\chi}}{\partial t} = -\overline{v}^* \frac{\partial \overline{\chi}}{\partial y} - \overline{w}^* \frac{\partial \overline{\chi}}{\partial z} + \frac{1}{\rho_0} \nabla \cdot M + \overline{S} \qquad (9)$$

The first and second terms on the right-hand side represent advection by residual mean motions (the Brewer-Dobson circulation), the third term represents flux convergence by wave motions analogous to the Eliassen-Palm flux in the TEM momentum equation, and the last term represents sources and sinks. Figure 16 shows calculations of the terms in the spherical coordinate version of equation (9) on model pressure levels using daily averaged output from run B from June to August. To first order, the balance is between the condensation sink (Figure 16a) and wave fluxes (Figure 16b), both of which are largest on any pressure level at about 75°S. Vertical transport (Figure 16c) supplies some moist air to the upper edge of the dehydration region but is insignificant elsewhere, and meridional transport (Figure 16d) is insignificant in this region. The actual tendency (Figure 16e) is negative below about 32 km not just within the vortex but outside it as well. Most of the water that has condensed out as polar temperatures drop has been supplied by wave motions, drying the region equatorward of 70°S (Figure 16c).

Zonal means are of course a crude way to regard the vortex, as its bounding latitude changes with both longitude and time. But the two largest terms are quite small equatorward of 65°S, suggesting that the water vapor supplied by flux convergence

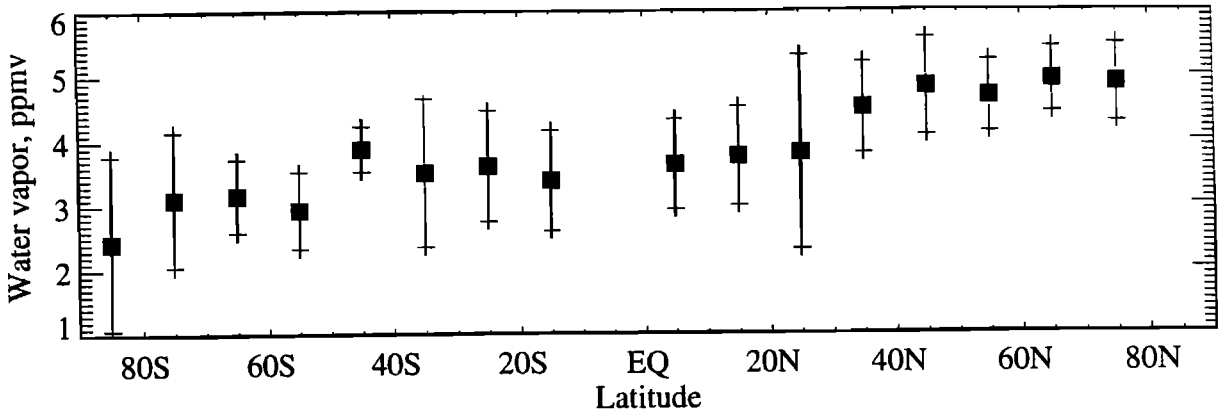

Figure 14. Latitude-binned water vapor data from ER-2 flights between 1987 and 1992, 400-450 K potential temperature. Bars show +/- 2σ of 5-min. averages. Data provided by K. Kelly, NOAA.

mostly came from within the vortex. Mixing ratio changes in midlatitudes are small, consistent with Figure 15.

Calculating tracer budgets. The predicted tendency, the balance of terms on the right hand side of (9) (Figures 16a to 16d), is shown in Figure 16f. Although the actual and predicted tendencies show general qualitative agreement and are within 0.01 ppmv day^{-1} below 27 km and south of 65°S, the difference between them, or residual, is significant in two regions. The relative error is greatest at 50°- 60°S where the predicted tendency is positive and the actual tendency is negative; the residual exceeds 0.01 ppmv day^{-1}. The residual itself is largest between 27 and 31 km south of 70°S but integrates to nearly zero over that region because the error of +0.02 ppmv day^{-1} at 31 km nearly balances a -0.02 ppmv day^{-1} error at 29 km. It would be useful to know why the residual is nonzero and why the errors at 29 and 31 km nearly cancel.

Equation (9) does not, of course, resemble the form of the continuity equation solved by the model, but the mathematical transformation from one to the other does not recognize the numerical factors which produce a residual. For example, errors in evaluating the wave flux term may arise from aliasing when calculating products like $v'\chi'$ and from finite differencing in calculating vertical derivatives. Other errors are attributable to sampling; model output consists of daily averages, masking higher-frequency fluctuations. Vertical derivatives in equation (9) are calculated with simple centered differences, which could lead to errors in regions of strong vertical gradient such as those at 30 km for water vapor. The transport code uses a more sophisticated approach to vertical transport.

Efforts to produce balanced tracer budgets are not new. *Mahlman and Moxim* [1976] discussed residuals which arise in evaluating tracer budgets on pressure surfaces when the model is cast in sigma coordinates; they showed that most of the error arose from the calculation of the vertical velocity and showed ways to improve this calculation. Using a similar technique and the same equation (9), *Randel et al.* [1994] calculated the budget of nitrous oxide in the CCM2 and found smaller but nonzero errors. Nitrous oxide does not experience the strong longitudinal and vertical variability of water vapor in the polar vortex, which partly explains why their balance was better than the one presented here. The residual could be reduced by spectrally truncating fields before calculating products, by rerunning the model and (1) writing output more often to reduce sampling errors, and (2) by writing out many more terms including a more precise form of the vertical velocity (P. Rasch, personal communication, 1993). These calculations show the difficulty of calculating budgets even when model fields are exactly known, as is true in a GCM.

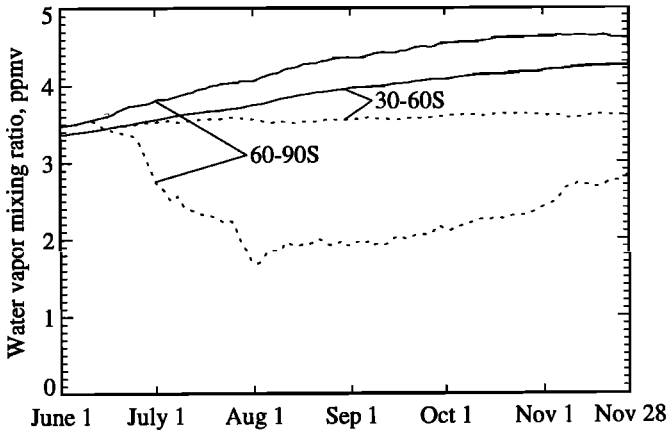

Figure 15. Time series of pressure-weighted mean mixing ratio (parts per million by volume) above 70 hPa for the control (solid lines) and no-dehydration (dotted lines) simulations, for the indicated area.

Timescale of midlatitude dehydration. If wave motions supply water vapor for dehydration within the lower stratospheric polar vortex, then one might expect to see transient drying associated with wave motions outside the vortex during the winter. But this is not the case; indeed, as is shown by Figure 16e, mixing ratios equatorward of 50°S actually increase during winter. How, then, is the dry lower stratosphere seen in Figure 4 to be explained?

The answer is that dryness in midlatitudes is produced later, when the vortex breaks down, and persists all year (especially in run A). Figure 17 clearly shows mixing ratios decreasing in midlatitudes beginning in November and reaching a minimum a few months later. It also suggests the propagation of dry air, as the minimum mixing ratio occurs later farther equatorward; the arrival of polar dry air in the 30°-40°S range (Figure 9b) coincides fortuitously with the dry air arriving from the tropics, resulting in temporal but not vertical agreement with SAGE II data [*McCormick et al.*, 1993]. The "ozone hole" simulations of *Mahlman et al.* [1994] show similar egress of low-ozone air in late spring. If dry, low-ozone air is traveling equatorward, it is not due to advection by the mean meridional

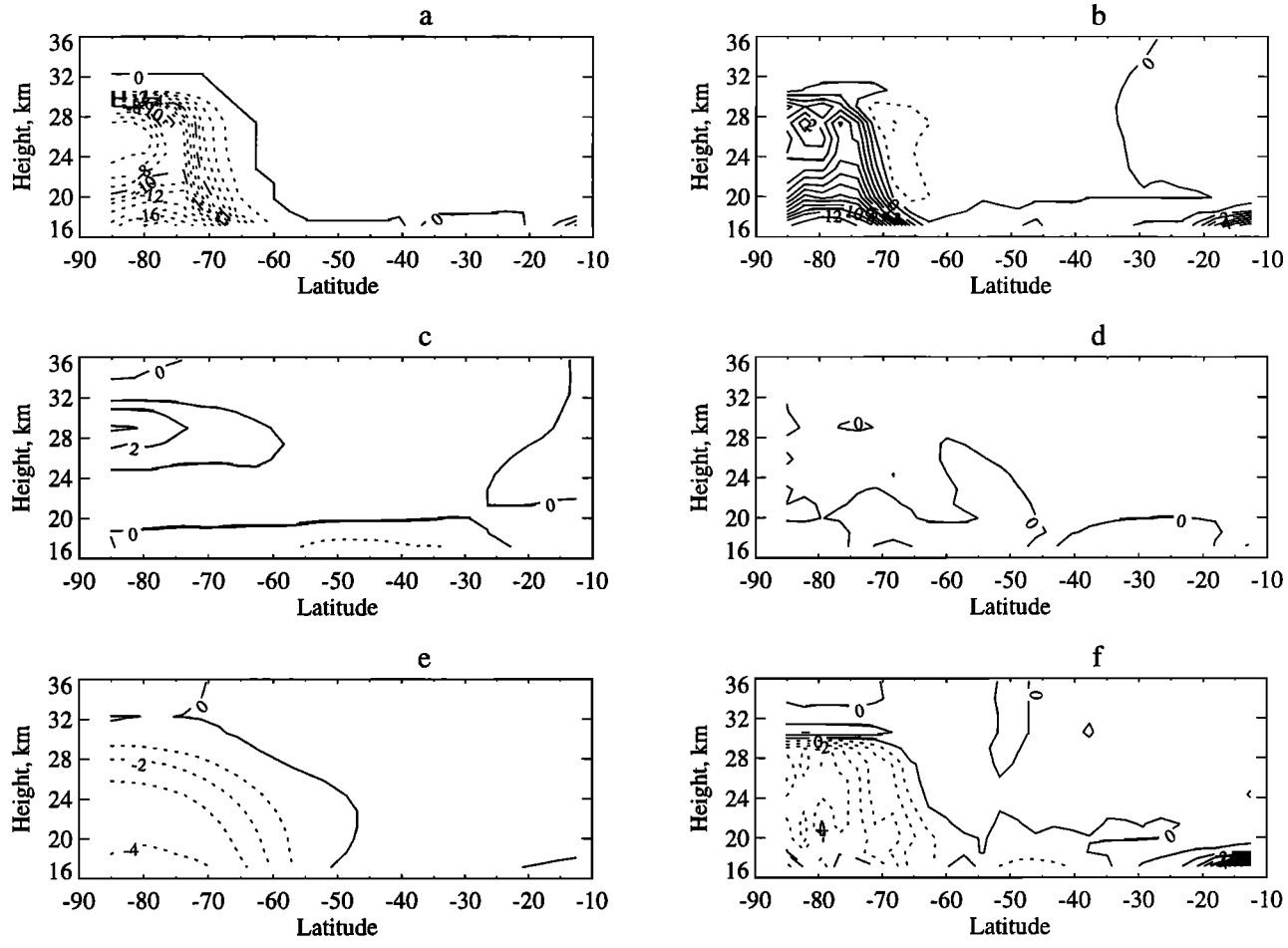

Figure 16. Terms in the water vapor tendency equation (eq. 9), for June-July-August of year 8, run B: (a) source+sink, (b) flux convergence, (c) vertical advection, (d) horizontal advection, (e) actual tendency, and (f) calculated tendency. Contour interval is 0.01 ppmv day^{-1}, negative contours are dotted, and the 0.05 and 0.1 ppmv day^{-1} contours are dashed.

circulation, which is poleward in the extratropical lower stratosphere, but to flux convergence.

The dryness in midlatitudes is also a consequence of the long times required for the lower stratosphere to reach equilibrium with the chemical source. For run B, the largest trend is in lower stratosphere, reaching a maximum of 0.28 ppmv year^{-1} in southern midlatitudes as it recovers from the excessive drying of run A. The initially dry stratosphere is moistened at first by influx at the tropical tropopause (since the mixing ratio there exceeds that of stratospheric air) and, more slowly, by the upper stratospheric methane conversion. In the northern hemisphere polar region, where dehydration does not occur, the lowest mixing ratios are also found in the lower stratosphere and increase slowly; in May, just before the re-

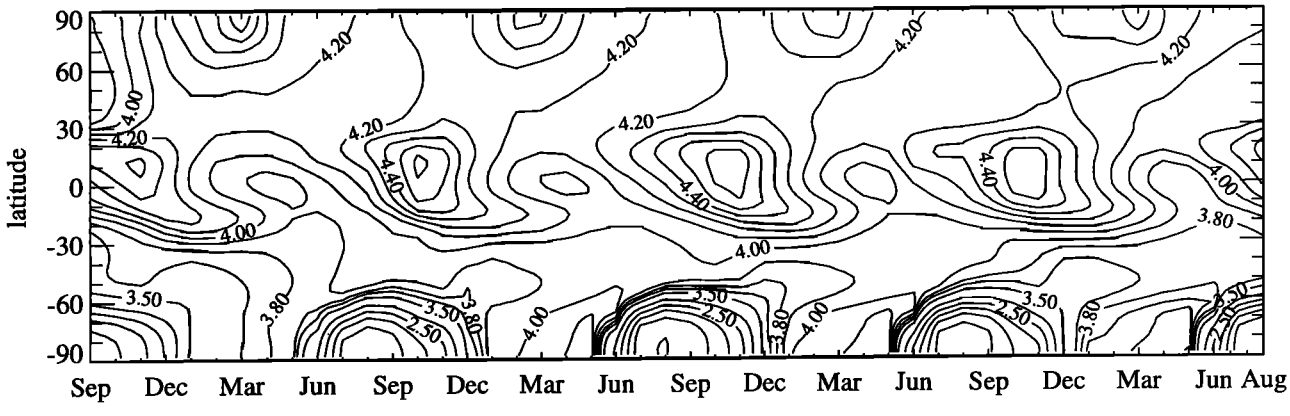

Figure 17. Evolution of monthly mean, zonal mean water vapor at 50 hPa for run B.

turn of dehydration to the southern polar region, run B has nearly identical mixing ratios in the northern and southern polar lower stratosphere near the end of the model run.

6. Discussion and Conclusions

General Results

The CCM2 adequately simulates some features of the observed methane and water vapor distributions and annual cycles (*Rasch et al.* [1995] discuss other trace gases in the CCM2). In the zonal mean, the shapes of the tracer isopleths are generally the same as observed; they bow upward in the tropics and are flattened in midlatitudes, where waves mix constituents quasi-isentropically [*Holton,* 1986]. As is shown in Figure 6, the zonal mean water vapor can be well reproduced in the CCM2, although values are mostly higher than observed.

The results presented here confirm that the photochemical source of water vapor has an important influence on the water vapor distribution even in the lower stratosphere; exchange with the troposphere is not the only process determining lower stratospheric water vapor. The importance of photochemistry is evident in Figure 3a, which shows a nearly linear increase in lower stratospheric mixing ratios with time, regardless of resolution. The mean mixing ratio at the tropical tropopause varied considerably during the 9 years of integration as the vertical resolution was changed; if influx from the troposphere were the only influence on lower stratospheric water vapor, average mixing ratios would decline when the model tropopause moved up and cooled in model year 5. Another implication of Figure 3a is that the lower stratosphere would respond very slowly to changes in the photochemical source. Adjustment in equilibrium water vapor should lag changes in methane by about a decade.

Modeling Water Vapor

The extreme sensitivity of water vapor saturation to temperature (Figure 1) makes it obvious that it is a very difficult tracer to model well. Two significant model deficiencies affect stratospheric water vapor: the representation of stratosphere-troposphere exchange processes and the impact of the polar temperature bias on southern hemisphere water vapor mixing ratios. In both cases, the temperature errors of the model are magnified in the water vapor field. Simulating physically correct tropical tropopause temperatures and vertical mass flux is a challenging and unsolved model problem.

Characteristics of stratosphere-troposphere exchange in the CCM2 were discussed by *Mote et al.* [1994], who found that the tropical tropopause seemed rather porous and permitted slightly too much water to enter the stratosphere. This is also the case even in simulations where the zonal mean water vapor resembles the observed (Figure 6); comparisons of simulated and observed area-averaged water vapor profiles (not shown) indicate that by the end of run B, water vapor is uniformly about 0.5-1.0 ppmv too large. The quantity $[H_2O]$-2*(1.5-$[CH_4]$), which *Jones et al.* [1986] define as "residual water" using 1.6 instead of 1.5 ppmv, provides an estimate of the mean water vapor mixing ratio of air entering the stratosphere. Residual water in the upper stratosphere at the end of run B is approximately 4 ppmv, compared with Jones et al's 2.7 ppmv.

Dehydration in the model's southern polar vortex tends to be much too intense due to the model's cold pole bias, a problem which has plagued general circulation models of the stratosphere from the beginning [*Smagorinsky et al.,* 1965]. As a result, southern hemisphere lower stratospheric mixing ratios can be considerably lower than observed mixing ratios all year. Steps taken to diminish the intensity of dehydration result in a marked improvement in southern midlatitude mixing ratios, which are low in southern spring but recover during the summer. Since GCMs generally have a cold pole bias, it seems likely that excessive dehydration would be a problem for others attempting to simulate stratospheric water vapor.

Water Vapor in the Midlatitude Lower Stratosphere

Observations [*McCormick et al.,* 1993; *Mastenbrook and Oltmans,* 1983] indicate that the seasonal cycle in midlatitude lower stratospheric water vapor is driven by the seasonal cycle at the tropical tropopause, as the minimum values appear in midlatitudes about a month or two after the tropical minimum. This is also the case in the model, but the annual subtropical maximum has greater influence on midlatitudes than the wintertime minimum (Figures 7 and 9), and the poleward flux of dry air is only weakly present. Dehydration at the tropical tropopause does, however, have a clear influence on the annual cycle in the tropics, where the signal propagates upward rather than poleward (Figure 10).

In the southern hemisphere, the midlatitude profile minimum is due to polar, not tropical, dehydration (Figures 9 and 17). But the minimum there occurs quite high (23 km); below that, the water vapor annual cycle is consistent with tropical influence. During southern winter, drying in the polar vortex has very limited influence on midlatitude mixing ratios (Figures 15, 16, and 17), but after the demise of the vortex the air dried by condensation in the vortex reduces mixing ratios in midlatitudes by less than 0.5 ppmv (Figure 17). The annual mean lower stratospheric water vapor in the CCM2 (not shown) has less interhemispheric variation than the ER-2 measurements (Figure 14), but that may be because the ER-2 measurements are not uniformly distributed throughout the year. The behavior of water vapor in southern midlatitudes has implications for the lively debate about the nature of the polar vortex.

The Southern Hemisphere Polar Vortex

Two contrasting views of the polar vortex have emerged, as summarized by *Randel* [1993]. The first view requires relatively large vertical velocities within the vortex which subject a large amount of air to chemical processing, the so-called "flowing processor" of *Tuck* [1989]. In the second view, the polar vortex is relatively isolated during the winter by large lateral potential vorticity gradients, and has only small vertical velocities, the so-called "containment vessel" of *McIntyre* [1989] and *Schoeberl et al.* [1992].

The wintertime (June-August) transformed-Eulerian mean vertical velocity within the polar vortex in the CCM2 varies strongly with height from 25 m day^{-1} below 20 km to 600 m day^{-1} at 50 km. *Tuck* [1989] postulated considerably larger descent rates in the lower polar vortex, so the flowing processor model does not describe the CCM2's polar vortex. The flux of dry air to midlatitudes is small in the CCM2 during June-August (Figures 16b, 16e, and 17) indicating that vortex air is reasonably well-contained until spring at least above 20 km.

Such a view of the polar vortex is consistent with other three-dimensional modeling studies. *Cariolle et al.* [1990, p. 1883] state that "[Above the 470K potential temperature level] the vision of the vortex acting as a containment vessel

holds, but below that level the vessel is apparently leaking!" Another simulation of the polar vortex using U.K. Meteorological Office winds and ideal tracers [*Chen et al.*, 1994] also indicates that the lower part of the vortex (below about 400 K) is easily and frequently disturbed by wave activity, while in the middle and upper stratosphere, the vortex is considerably more isolated.

Air dried by fallout of ice crystals from PSCs would also have low ozone amounts due to PSC processing, and any leakage of the "containment vessel" would be identifiable as low water vapor, low ozone air. The simulation by *Cariolle et al.* [1990] of ozone decrease due to heterogeneous chemistry within the polar vortex showed springtime midlatitude ozone decrease between 390 K and 470 K. They also showed a tongue of dry air extending to about 30°S between 440 and 480 K. It should be noted that their temperature bias is at least as severe as that of CCM2, yet they show no dehydration above 40 hPa; they must have artificially limited the magnitude of dehydration, but did not discuss how. *Mahlman et al.* [1994] showed similar results in a multiyear simulation; air depleted in ozone entered midlatitudes after the breakup of the polar vortex in about December.

Acknowledgments. The author wishes to acknowledge helpful comments on the manuscript by James Holton, Jerry Mahlman, and Mark Schoeberl, and discussions with Byron Boville, Philip Rasch, and Adrian Tuck. Ellis Remsberg, Er-woon Chiou, and Ken Kelly kindly provided (respectively) the LIMS data for Figure 5a, the SAGE II data for Figure 5b, and the ER-2 data for Figure 14. This work was supported by NASA Global Change Fellowship NGT 30076.

References

Allam, R.J., and A.F. Tuck, Transport of water vapour in a stratosphere-troposphere general circulation model, I, Fluxes, *Q. J. R. Meteorol. Soc., 110,* 321-356, 1984.

Andrews, D.G., J.R. Holton, and C.B. Leovy, *Middle Atmosphere Dynamics*. Academic, San Diego, Calif., 489 pp, 1987.

Brewer, A.W., Evidence for a world circulation provided by the measurement of helium and water vapour distribution in the stratosphere, *Quart. J. Roy. Meteor. Soc., 75,* 351-363, 1949.

Cariolle, D., A. Lasserre-Bigorry, and J.F. Royer, A general circulation model simulation of the springtime Antarctic ozone decrease and its impact on mid-latitudes, *J. Geophys. Res. 95,* 1883-1898, 1990.

Chen, P., J.R. Holton, A. O'Neill, and R. Swinbank, Quasi-horizontal transport and mixing in the Antarctic stratosphere, *J. Geophys. Res. 99,* 16,851-16,866, 1994.

Chiou, E.W., M.P. McCormick, L.R. McMaster, W.P. Chu, J.C. Larsen, D. Rind, and S. Oltmans, Intercomparison of stratospheric water vapor observed by satellite experiments: Stratospheric Aerosol and Gas Experiment II versus Limb Infrared Monitor of the Stratosphere and Atmospheric Trace Molecule Spectroscopy, *J. Geophys. Res., 98,* 4875-4888, 1993.

Ellsaesser, H.W., Water budget of the stratosphere, in Third CIAP Conference, *Rep. DOT-TSC-OST-74-15,* pp. 273-283, U.S. Dep. of Transp., Washington, D.C., 1974.

Ellsaesser, H.W., Comment on "The distribution of water vapor in the stratosphere" by J.E. Harries, *Rev. Geophys., 15,* 501, 1977.

Ellsaesser, H.W., Stratospheric water vapor, *J. Geophys. Res., 88,* 3897-3906, 1983.

Frederick, J.E., and A.R. Douglass, Atmospheric temperatures near the tropical tropopause: Temporal variations, zonal asymmetry and implications for stratospheric water vapor, *Mon. Weather Rev. , 111,* 1397-1403, 1983.

Garcia, R.R., and B.A. Boville, "Downward control" of the mean meridional circulation and temperature distribution of the polar winter stratosphere, *J. Atmos. Sci.,* in press, 1995.

Garcia, R.R., and S. Solomon, A numerical model of the zonally averaged dynamical and chemical structure of the middle atmosphere, *J. Geophys. Res., 88,* 1379-1400, 1983.

Hack, J.J., Parameterization of moist convection in the National Center for Atmospheric Research Community Climate Model (CCM2), *J. Geophys. Res., 99,* 5551-5568, 1994.

Hack, J.J., B.A. Boville, B.P. Briegleb, J.T. Kiehl, P.J. Rasch, D.L. Williamson, Description of the NCAR Community Climate Model (CCM2), *Technical Note NCAR/TN-382+STR,* National Center for Atmospheric Research, Boulder, Colorado, 1993.

Hansen, A.R., and G.D. Robinson, Water vapor and methane in the upper stratosphere: An examination of some of the Nimbus 7 measurements, *J. Geophys. Res., 94,* 8474-8484, 1989.

Harries, J.E., The distribution of water vapor in the stratosphere, *Rev. Geophys., 14,* 565-575, 1976.

Harwood, R.S., E.S. Carr, L. Froidevaux, R.F. Jarnot, W.A. Lahoz, C.L. Lau, G.E. Peckham, W.G. Read, P.D. Ricaud, R.S. Suttie, and J.W. Waters, Springtime stratospheric water vapour in the southern hemisphere as measured by MLS, *Geophys. Res. Lett., 20,* 1235-1238, 1993.

Holton, J.R., Troposphere-stratosphere exchange of trace constituents: The water vapor puzzle, in *Dynamics of the Middle Atmosphere,* edited by J.R. Holton and T. Matsuno, pp. 369-385, Terra. Scientific, Tokyo, 1984.

Holton, J.R., Meridional distribution of stratospheric trace constituents, *J. Atmos. Sci., 43,* 1238-1242, 1986.

Jones, R.L., A. Pyle, J.E. Harries, A.M. Zavody, J.M. Russell III, and J.C. Gille, The water vapour budget of the stratosphere studied using LIMS and SAMS satellite data, *Q. J. R. Meteorol. Soc., 112,* 1127-1144, 1986.

Kelly, K.K., A.F. Tuck, D.M. Murphy, M.H. Proffitt, D.W. Fahey, R.L. Jones, D.S. McKenna, M. Loewenstein, J.R. Podolske, S.E. Strahan, G.V. Ferry, K.R. Chan, J.F. Vedder, G.L. Gregory, W.D. Hypes, M.P. McCormick, E.V. Browell, and L.E. Heidt, Dehydration in the lower Antarctic stratosphere during late winter and early spring, 1987, *J. Geophys. Res., 94,* 11,317-11,357, 1989.

Kelly, K.K., A.F. Tuck, L.E. Heidt, M. Loewenstein, J.R. Podolske, S.E. Strahan, and J.F. Vedder, A comparison of ER-2 measurements of stratospheric water vapor between the 1987 Antarctic and 1989 Arctic airborne missions, *Geophys. Res. Lett., 17,* 465-468, 1990.

Kelly, K.K., M. H. Proffitt, K.R. Chan, M. Loewenstein, J.R. Podolske, S.E. Strahan, J.C. Wilson, and D. Kley, Water vapor and cloud water measurements over Darwin during the STEP 1987 tropical mission, *J. Geophys. Res., 98,* 8713-8724, 1993.

Kley, D., E. J. Stone, W.R. Henderson, J.W. Drummond, W.J. Harrop, A.L. Schmeltekopf, T.L. Thompson, and R.H. Winkler, In situ measurements of the mixing ratio of water vapor in the stratosphere, *J. Atmos. Sci., 36,* 2513-2524, 1979.

Kley, D., A.L. Schmeltekopf, K. Kelly, R. H. Winkler, T.L. Thompson, and M. McFarland, Transport of water through the tropical tropopause, *Geophys. Res. Lett., 9,* 617-620, 1982.

Le Texier, H., S. Solomon, and R.R. Garcia, The role of molecular hydrogen and methane oxidation in the water vapour budget of the stratosphere, *Q. J. R. Meteor. Soc. 114,* 281-295, 1988.

Mahlman, J.D., and W.J. Moxim, A method for calculating more accurate budget analyses of "sigma" coordinate model results, *Mon. Weather Rev., 104,* 1102-1106, 1976.

Mahlman, J.D., J.P. Pinto, and L.J. Umscheid, Transport and dynamical effects of the Antarctic ozone hole: A GFDL "SKYHI" model experiment, *J. Atmos. Sci., 51,* 489-508, 1994.

Mastenbrook, H.J., Water vapor distribution in the stratosphere and high troposphere, *J. Atmos. Sci., 25,* 299-311, 1968.

Mastenbrook, H.J., Water vapor measurements in the lower stratosphere, *Can. J. Chem., 52,* 1527-1531, 1974.

Mastenbrook, H.J., and S.J. Oltmans, Stratospheric water vapor variability for Washington, DC/ Boulder, CO: 1964-1982, *J. Atmos. Sci., 40,* 2157-2165, 1983.

McCormick, M.P., and E.-W. Chiou, Climatology of water vapor in the upper troposphere and lower stratosphere determined from SAGE II

observations, in *Reprints of the 5th Symposium on Global Change Studies,* American Meteorological Society, Boston, Mass., 1994.

McCormick, M.P., H.M. Steele, P. Hamill, W.P. Chu, and T.J. Swissler, Polar stratospheric cloud sightings by SAM II, *J. Atmos. Sci., 39,* 1387-1397, 1982.

McCormick, M.P., E. W. Chiou, L.R. McMaster, W.P. Chu, J.C. Larsen, D. Rind, and S. Oltmans, Annual variations of water vapor in the stratosphere and upper troposphere observed by the Stratospheric Aerosol and Gas Experiment II, *J. Geophys. Res., 98,* 4867-4874, 1993.

McIntyre, M.E., On the Antarctic ozone hole, *J. Atmos. Terrest. Phys., 51,* 29-43, 1989.

Molina, M.J., T.-L. Tso, L.T. Molina, and F.C.-Y. Wang, Antarctic stratospheric chemistry of chlorine nitrate, hydrogen chloride, and ice: Release of active chlorine, *Science, 238,* 1253-1257, 1987.

Mote, P.W., J.R. Holton, J.M. Russell III, and B.A. Boville, A comparison of observed (HALOE) and modeled (CCM2) methane and stratospheric water vapor. *Geophys. Res. Lett., 20,* 1419-1422, 1993.

Mote, P.W., J.R. Holton, and B.A. Boville, Characteristics of stratosphere-troposphere exchange in a general circulation model, *J. Geophys. Res., 99,* 16,815-16,829, 1994.

Mote, P.W., K.M. Rosenlof, J.R. Holton, R.S. Harwood, and J.W. Waters, Seasonal variations of water vapor in the tropical lower stratosphere, *Geophys. Res. Lett.,* in press, 1995.

Newell, R.E., and S. Gould-Stewart, A stratospheric fountain?, *J. Atmos. Sci., 38,* 2789-2796, 1981.

Randel, W.J., Ideas flow on Antarctic vortex, *Nature, 364,* 105-106, 1993.

Randel, W.J., B.A. Boville, J.C. Gille, P.L. Bailey, S.T. Massie, J.B. Kumer, J.L. Mergenthaler, and A.E. Roche, Simulation of stratospheric N_2O in the NCAR CCM2: Comparison with CLAES data and global budget analyses, *J. Atmos. Sci., 51,* 2834-2845, 1994.

Rasch, P.J., and D.L. Williamson, The sensitivity of a general circulation model climate to the moisture transport formulation, *J. Geophys. Res., 96,* 13123-13137, 1991.

Rasch, P.J., X. Tie, B.A. Boville, and D.L. Williamson, A three-dimensional transport model for the middle atmosphere, *J. Geophys. Res.,* in press, 1995.

Remsberg, E.E., J.M. Russell III, L.L. Gordley, J.C. Gille, and P.L. Bailey, Implications of the stratospheric water vapor distribution as determined from the Nimbus 7 LIMS experiment, *J. Atmos. Sci., 41,* 2934-2945, 1984.

Remsberg, E.E., K.V. Haggard, and J.M. Russell III, Estimation of synoptic fields of middle atmosphere parameters from Nimbus 7 LIMS profile data, *J. Atmos. and Oceanic Technol., 7,* 689-705, 1990a.

Remsberg, E.E., J.M. Russell III, and C.-Y. Wu, An interim reference model for the variability of the middle atmospheric water vapor distribution. *Adv. Space. Res., 10 (6),* 51-64, 1990b.

Rind, D., E.-W. Chiou, W. Chu, S. Oltmans, J. Lerner, J. Larsen, M.P. McCormick, and L. McMaster, Overview of the Stratospheric Aerosol and Gas Experiment II water vapor observations: method, validation and data characteristics, *J. Geophys. Res., 98,* 4835-4856, 1993.

Robinson, G.D., and M.G. Atticks Schoen, The formation and movement in the stratosphere of very dry air, *Q. J. R. Meteorol. Soc., 113,* 653-679, 1987.

Russell, J.M. III, J.C. Gille, E.E. Remsberg, L.L. Gordley, P.L. Bailey, H. Fisher, A. Girard, S.R. Drayson, W.F.J. Evans, and J.E. Harries, Validation of water vapor results measured by the limb infrared monitor of the stratosphere experiment on Nimbus 7, *J. Geophys. Res. 89,* 5115-5124, 1984.

Schoeberl, M.R., L.R. Lait, P.A. Newman and J.E. Rosenfield, The structure of the polar vortex, *J. Geophys. Res., 97,* 7859-7882, 1992.

Selkirk, H.B., The tropopause cold trap in the Australian monsoon during STEP/AMEX 1987, *J. Geophys. Res., 98,* 8591-8610, 1993.

Smagorinsky, J., S. Manabe, and J.L. Holloway, Numerical results from a nine-level general circulation model of the atmosphere, *Mon. Weather Rev., 93,* 727-768, 1965.

Stanford, J.L., Possible sink for stratospheric water vapor at the winter Antarctic pole, *J. Atmos. Sci., 30,* 1431-1476, 1973.

Tuck, A.F., Synoptic and chemical evolution of the Antarctic vortex in the late winter and early spring, *J. Geophys. Res., 94,* 11,687-11,737, 1989.

Tuck, A.F., J.M. Russell III, and J.E. Harries, Stratospheric dryness: Antiphased desiccation over Micronesia and Antarctica, *Geophys. Res. Lett., 20,* 1227-1230, 1993.

Watterson, I.G., and A.F. Tuck, A comparison of the longitudinal distributions of polar stratospheric clouds and temperatures for the 1987 Antarctic spring. *J. Geophys. Res., 94,* 16,511-16,525, 1989.

P. Mote, Department of Meteorology, King's Buildings, University of Edinburgh, Edinburgh EH9 3JZ, Scotland. (e-mail: mote@met..ed.ac.uk)

Received December 12, 1993; revised July 13, 1994;
accepted August 30, 1994.